

Dynamics of a Mixed Monolayer Consisting of a Soluble Amphiphile and Its Insoluble 2D Condensing Homologue

V. B. Fainerman,[†] D. Vollhardt,^{*,‡} and S. Siegel[‡]

Max-Planck Institute of Colloids and Interfaces, D-14424 Potsdam/Golm, Germany, and Medical Physicochemical Center, Donetsk Medical University, 16 Ilych Avenue, Donetsk 340003, Ukraine

Received: January 9, 2002; In Final Form: March 26, 2002

The dynamics of a mixed monolayer consisting of a soluble tailored amphiphile *N*-decyl- γ -hydroxybutyric acid amide (C₁₀NH) and its insoluble condensing homologue *N*-tetradecyl- γ -hydroxybutyric acid amide (C₁₄NH) are experimentally and theoretically studied. Single-component and mixed monolayers of the soluble C₁₀NH and the insoluble C₁₄NH are studied experimentally, and the results are compared with theoretical predictions. For some theoretical models, equations of state for mixed monolayers of an insoluble and a soluble homologue and the adsorption isotherm equation for soluble amphiphile are derived. Assuming diffusion kinetics for the desorption of the soluble component during the compression of the mixed monolayer, a new equation for the surface concentration (adsorption) of the soluble amphiphile allows one to analyze this value with dependence on the conditions of the monolayer compression, concentration, and other parameters. The influence of the nonideality of the mixture on the shift of the area value per molecule of the insoluble amphiphile, which corresponds to the commencement of the two-dimensional condensation in the monolayer, is theoretically treated. The theoretical predictions are in a satisfactory agreement with the experiments. It is shown that the account for the nonideality in the mixture of amphiphiles is important for the qualitative and quantitative analysis of the formation of domains in the mixed monolayer.

Introduction

Equilibrium and dynamic behavior of mixed monolayers of soluble and insoluble amphiphiles at fluid/liquid interfaces play an important role in various technologic and biologic processes and, therefore, have been studied in numerous publications.^{1–19} In a recent review,²⁰ an analysis is given of the main theoretical methods used for describing mixed monolayers, with special emphasis to systems where the insoluble component of the monolayer is capable of two-dimensional condensation. In this case, (i) the condensation of the insoluble component essentially affects the adsorption behavior of the soluble amphiphile and (ii) the adsorption of the soluble component affects the 2D condensation of the insoluble species.

To understand the complexity which arises in the description of the equilibrium established in the mixed monolayers of soluble and insoluble amphiphiles, this system can be compared with mixed adsorbed monolayers of soluble surfactants at liquid interfaces. The adsorption behavior of mixed surfactant solutions at liquid interfaces was considered in many papers, whereas theoretic models were reviewed in refs 21–25. All models proposed so far dealt with the prediction of surface or interfacial tensions of mixed solutions from the known characteristics of the single compounds. Therefore, in all equations of state proposed for mixed surface layers, the isotherm parameters of the pure compounds were involved (usually the number of these parameters is 2 or 3). To match the experimental data with theoretical predictions, an additional parameter was introduced

to account for the mutual influence of the monolayer components. This imposes certain restrictions on the capabilities of these approaches to predict the adsorption behavior of surfactant mixtures.

In ref 23, an attempt was made to calculate theoretically all parameters of the equation of state and adsorption isotherm for a mixture of (ionic or nonionic) surfactants. The areas per molecule were calculated from the bonding lengths and angles for surfactants having compact hydrophilic headgroups and via Monte Carlo simulations for surfactants having flexible, polymer-like hydrophilic heads. The intermolecular interaction parameters were also to be calculated theoretically. However, it is impossible to calculate reliable theoretical estimates of the difference between the chemical potentials of the component in the bulk and at the surface which determines the adsorption activity of the surfactant.

Two-dimensional aggregation in the monolayer makes the theoretical analysis still more complicated. It seems therefore that approximate additivity-based models, similar to that proposed recently in ref 26 to describe the mixed monolayer of soluble sodium dodecyl sulfate and less soluble dodecanol, could be more analytically treatable than rigorous models.

For mixed insoluble monolayers, the problem becomes much more complicated. To study the dynamic behavior of the mixed monolayer of a soluble and an insoluble amphiphile, two methods are of common use. In the first one, namely, the penetration, at first the insoluble monolayer with some predefined coverage is formed, and then, the dynamics of the adsorption (penetration) of the soluble amphiphile into this monolayer is studied. It was particularly found that the penetration of the soluble amphiphile results in the fact that the

* To whom correspondence should be addressed.

[†] Donetsk Medical University.

[‡] Max-Planck Institute of Colloids and Interfaces.

insoluble component starts to undergo the condensation at a lower monolayer coverage as compared with that occurring in its single monolayer.^{17,19,20} Another experimental method, in which the diluted monolayer of the insoluble amphiphile is brought to the equilibrium with the solution of the soluble amphiphile and then the mixed monolayer is compressed, is a much more difficult task. The attempts to analyze such a system for the case of two-dimensional condensation of the insoluble component were made in refs 20 and 21. However, it was presupposed that the soluble amphiphile cannot desorb from the monolayer (the monolayer is conserved).

In the present study, we make an attempt to analyze the behavior of the compressible mixed monolayer without any simplifying assumptions in the framework of the theory of the adsorption/desorption diffusion kinetics. It is shown that the new model, while exhibiting satisfactory agreement with the experimental results, also elucidates the subtle mechanism of the effect produced by the soluble amphiphile on the condensation of the insoluble component. It should be noted that the two experimental methods and the two types of the models, while being important methods for the analysis of mixed monolayers, are also applicable to actual biologic and technologic processes, e.g., compression/expansion of bio-membranes, coalescence, or dispersion of emulsions. Therefore, the theoretical model of the compressible mixed monolayer proposed here is also important in a general sense.

Theory

One-Component Monolayers. There exist some models which describe the equilibrium adsorption behavior of soluble amphiphiles. The equation of state and adsorption isotherm for the Frumkin model (which becomes the Langmuir model for $a = 0$) are^{21,28}

$$-\frac{\Pi\omega}{RT} = \ln(1 - \theta) + a\theta^2 \quad (1)$$

$$bc = \frac{\theta}{1 - \theta} \exp(-2a\theta) \quad (2)$$

where R is the gas law constant, T is the temperature, $\Pi = \gamma_0 - \gamma$ is the surface pressure, γ_0 and γ are the surface tension of solvent and solution, respectively, ω is the molar area, θ is the surface coverage, $\theta = \Gamma\omega$, Γ is the adsorption, c is the bulk concentration, a is the intermolecular interaction constant, and b is the adsorption equilibrium constant. For the values of $a \geq 2$, the critical state of the monolayer (the coexistence between the gaseous and condensed states) can exist.^{28–30} Therefore, the theory which assumes the formation of the aggregates in the monolayer should be most appropriate for such systems.^{31,32}

The model for aggregation in the adsorption layer with the arbitrary aggregation number n is described by the following equation of state and adsorption isotherm^{21,27}

$$-\frac{\Pi\omega}{RT} = \ln\{1 - \Gamma_1\omega[1 + (\Gamma_1/\Gamma_c)^{n-1}]\} \quad (3)$$

$$bc = \frac{\Gamma_1\omega}{\{1 - \Gamma_1\omega[1 + (\Gamma_1/\Gamma_c)^{n-1}]\}^{\omega_1/\omega}} \quad (4)$$

Here Γ_1 and Γ_c are the partial and critical adsorption of monomers, respectively, and the average molar area ω should be expressed via the equation

$$\frac{\omega}{\omega_1} = \frac{1 + n(\Gamma_1/\Gamma_c)^{n-1}}{1 + (\Gamma_1/\Gamma_c)^{n-1}} \quad (5)$$

where ω_1 is the molar area of monomers.

The insoluble monolayers of amphiphiles often demonstrate the two-dimensional phase transition from a fluid (LE) to a condensed (LC) state, which corresponds to the break point in the surface pressure (Π) – area per molecule (A) isotherm. The two-dimensional phase transition (LE \rightarrow LC) for $A \leq A_c$ leads to the formation of condensed aggregates in the monolayer characterized by the aggregation number $n \gg 1$ ($n \rightarrow \infty$). If the monolayer consists only of monomers and large aggregates, the equation of state for the monolayer at $A \leq A_c$ is^{33–35}

$$\Pi = \frac{kT(A/A_{c\Pi})^2}{A - \Omega_1[1 + \epsilon((A/A_{c\Pi})^2 - 1)]} - \Pi_{\text{coh}} \quad (6)$$

where

$$A_{c\Pi} = A_c \exp\left(\frac{(\Pi - \Pi_c)\epsilon\omega_1}{RT}\right) \quad (7)$$

Here k is the Boltzmann constant, Ω_1 and ω_1 are the partial molecular and molar area for monomers, respectively ($\Omega_1 = \omega_1/N$), $A = 1/N\Gamma$ is the area per molecule, N is the Avogadro's number, Π_{coh} is the cohesion pressure, Γ is the surface concentration (adsorption), $\theta = \Omega_1/A = N\Gamma\Omega_1$ is the monolayer coverage, ϵ is a correcting factor which accounts for the decrease of the area per one molecule during the aggregation, and $A_c = 1/N\Gamma_c$ is the molecular area which corresponds to the main phase transition point, i.e., at $\Pi = \Pi_c$. For $A \geq A_c$, eq 7 becomes the Volmer equation for monomers^{35,36}

$$\Pi = \frac{kT}{A - \Omega_1} - \Pi_{\text{coh}} = \frac{RT}{1 - \theta} - \Pi_{\text{coh}} \quad (8)$$

Mixed Monolayer of Homologues in the Precritical Region. The theoretical description of the equilibrium of the mixture of a soluble surfactant and a Langmuir monolayer becomes less complicated if the partial molar areas of the two components are approximately equal to each other. The equation of state which, for monolayers formed by the mixture of insoluble and soluble components, expresses both the dependence of the surface pressure on the adsorption of the soluble surfactant, similarly to the eq 1, and the surface pressure dependence on the surface concentration of the insoluble component, similarly to the Volmer equation eq 8, is unfortunately not available. Therefore, for low adsorption of the soluble component, the generalized Volmer equation can be used to describe the two components of the monolayer, whereas for low adsorption of the insoluble component, the generalized Szyszkowski–Langmuir equation is employed.²⁰

The generalized Szyszkowski–Langmuir equation of state and the adsorption isotherm equation for the mixture of two homologues, the insoluble (1) and soluble (2) ones, when 2D aggregation does not occur are²⁰

$$\Pi = -\frac{RT}{\omega} \ln(1 - \theta_1 - \theta_2) \quad (9)$$

$$bc = \frac{\theta_2}{1 - \theta_1 - \theta_2} \quad (10)$$

where $\omega = \omega_2 = \omega_1$ is the molar area of the soluble and

insoluble amphiphiles. These equations could be rearranged into a more convenient form:

$$\Pi = \frac{RT}{\omega} \ln \frac{(1 + bc)}{(1 - \theta_1)} \quad (11)$$

$$\Gamma_2 = \frac{1 - \theta_1}{\omega} \frac{bc}{1 + bc} \quad (12)$$

It follows from eq 11 that the variation (jump) of the monolayer surface pressure which arises because of the adsorption of soluble surfactant, that is, the difference between the pressures of the mixed monolayer and the pure insoluble monolayer $\Delta\Pi$, does not depend on θ_1 but depends on the value of bc only:

$$\Delta\Pi = (RT/\omega) \ln(1 + bc) \quad (13)$$

According to the isotherm equation, eq 12, the monolayer coverage by the soluble component in the presence of the insoluble component decreases proportionally to $(1 - \theta_1)$. Therefore, the θ_2 value, which corresponds to some $\Delta\Pi$ values for the mixed monolayer, is lower than the θ_2 value that corresponds to the same $\Delta\Pi$ for the case when the monolayer does not contain the insoluble amphiphile.

For low adsorption of the soluble component, the generalized Volmer equation can be used to describe two or more components of the monolayer:^{20,21}

$$\Pi = RT \frac{\sum_i \Gamma_i}{1 - \sum_i \Gamma_i \omega_i} - \Pi_{\text{coh}} \quad (14)$$

For $A \geq A_c$ and for the two components 1 and 2, eq 14 can be transformed into

$$\Pi = RT \frac{\Gamma_2 + 1/NA}{1 - \omega_2 \Gamma_2 - \Omega_1/A} - \Pi_{\text{coh}} \quad (15)$$

Using eq 12, one can express the actual value of the adsorption of soluble amphiphile 2 in eq 15 by its equilibrium value in the single-component solution $\Gamma_2^* = (1/\omega_2)bc/(1 + bc)$. Finally, one obtains from eq 15

$$\Pi = RT \frac{\Gamma_2^*(1 - \Omega_1/A) + 1/NA}{1 - \omega_2 \Gamma_2^*(1 - \Omega_1/A) - \Omega_1/A} - \Pi_{\text{coh}} \quad (16)$$

Note that eq 15 covers the cases of both equilibrium and nonequilibrium adsorption of the component 2, whereas eq 16 can be used only if equilibrium adsorption takes place.

In rigorous development, the application of the generalized Volmer equation for the two components (both the soluble 2 and insoluble 1 ones) results in the modified adsorption isotherm equation for component 2. It was shown in ref 20 that the simultaneous solution of eq 14 and the Pethica equation^{1,2}

$$\left(\frac{\partial \Pi}{\partial \ln c} \right)_{\theta_1} = \frac{RT\Gamma_2}{(1 - \theta_1)} \quad (17)$$

results in the adsorption isotherm equation for the soluble amphiphile

$$bc = \left(\frac{\theta_2}{1 - \theta_1 - \theta_2} \right)^{1/(1 - \theta_1)} \exp \left[\frac{\theta_2}{(1 - \theta_1)(1 - \theta_1 - \theta_2)} \right] \quad (18)$$

where $\theta_1 = \Omega_1/A$ and $\theta_2 = \Gamma_2\omega_2$ and for $\theta_1 = 0$ the isotherm equation which follows from eq 18:

$$bc = \frac{\theta_2}{1 - \theta_2} \exp \left(\frac{\theta_2}{1 - \theta_2} \right) \quad (19)$$

which differs from eq 2 for $a = 0$ by an exponential factor.

Mixed Monolayer in the Transcritical Region. Considering now the area range $A \leq A_{\text{cm}}$, one can see that the form of the equation of state and the adsorption isotherm depends on the type of the formed aggregates^{17–20} and also on the model used (generalized Szyszkowski or generalized Volmer equation). The subscript “cm” at the critical area value is introduced to denote that this value in the mixed monolayer can be different from that for the single monolayer. If infinitely large aggregates of the insoluble homologue are formed, the equation of state of mixed monolayer (eq 9) becomes^{26,27}

$$\Pi = - \frac{RT(\theta_{\text{cm}} + \theta_2)}{\omega(\theta_1 + \theta_2)} \ln(1 - \theta_1 - \theta_2) \quad (20)$$

whereas the adsorption isotherm equation for the soluble component remains approximate the same, see eq 10 or 12, if $(\theta_{\text{cm}} + \theta_2)/(\theta_1 + \theta_2) \cong 1$.²⁶

Provided that the aggregates consist mainly of the insoluble homologue, for Volmer’s model, the equation of state for the arbitrary value of the adsorption of component 2 becomes²⁰

$$\Pi = RT \frac{\Gamma_2 + (1/NA_{\text{cm}})(A/A_{\text{cm}})}{1 - \omega_2 \Gamma_2 - \Omega_1/A} - \Pi_{\text{coh}} \quad (21)$$

If the process of monolayer compressing is slow enough and adsorption of component 2 is in equilibrium with the solution, with this equilibrium governed by eq 12, then eq 21 transforms to

$$\Pi = RT \frac{\Gamma_2^*(1 - \Omega_1/A) + (1/NA_{\text{cm}})(A/A_{\text{cm}})}{1 - \omega_2 \Gamma_2^*(1 - \Omega_1/A) - \Omega_1/A} - \Pi_{\text{coh}} \quad (22)$$

The adsorption isotherm equation corresponding to the equation of state (eq 21) can be derived from the simultaneous solution of eqs 21 and 17. This leads to the adsorption isotherm equation for component 2 in the range $A \leq A_{\text{cm}}$.²⁰

$$bc = \left(\frac{\theta_2}{1 - \theta_1 - \theta_2} \right)^{(1 - \theta_1 + \theta_{1c})/(1 - \theta_1)} \exp \left[\frac{\theta_2(1 - \theta_1 + \theta_{1c})}{(1 - \theta_1)(1 - \theta_1 - \theta_2)} \right] \quad (23)$$

It is seen that in absence of aggregation (corresponding to the condition $\theta_{1c} = \theta_1$) the adsorption isotherm equation (eq 23) becomes identical to eq 18 which is valid in the precritical region.

Therefore, the following options exist for the theoretical description of either the equilibrium or nonequilibrium mixed monolayer in the precritical ($A \geq A_{\text{cm}}$) or transcritical ($A \leq A_{\text{cm}}$) range, based on the following:

(I) The generalized Szyszkowski–Langmuir model, eqs 11 and 12 and 20 and 12 for the precritical and transcritical range, respectively

(II) The combined Langmuir and Volmer’s models, eqs 15 and 12 and 21 and 12, respectively

(III) The generalized Volmer’s–Pethica’s model, eqs 15 and 18 and 21 and 23, respectively.

Dependence of the A_c Value on the Soluble Component.

For the formation of aggregates in the mixed monolayer, both components affect the value of the critical adsorption of the aggregate formation (or A_c).^{17–20} To calculate the A_c value for the formation of mixed aggregates, one should know the ratio of the components in the domain.^{18,20} However, in most of the cases known so far, mixed aggregates are not formed, and therefore, in the mixed monolayer, the domains consist of component 1 only. In this case, the presence of component 2 results in the decrease of the fraction of the free surface of the monolayer. Calculating the sum of the adsorptions (surface concentrations) of the two components, one obtains a simple expression for A_{cm} , i.e., the critical area per one molecule of insoluble amphiphile in the mixed monolayer.^{19,20}

$$\frac{1}{NA_{cm}} = \frac{1}{NA_c} - \Gamma_2 \quad (24)$$

or, if homologues are considered, this can be expressed by the monolayer coverages

$$\theta_{cm} = \theta_c - \theta_2 \quad (25)$$

Equations 24–25 were shown in refs 17–20 to give quite satisfactory correspondence with experimental results for some systems.

It is possible to derive a more general expression for the critical area A_{cm} in the mixed monolayer on the basis of eq 25. Possibly, the most correct procedure is to compare and to add the activities of the components in the single and mixed monolayer, rather than the adsorptions (or coverages) of the components. The activity of the insoluble component in the monolayer is given by the $x_1\gamma_1$ value, where x_1 is the molar fraction of the component, and the activity coefficient γ_1 , arising from nonideality of the mixing enthalpy, depends on the composition of the monolayer^{37,38} for the single-component monolayer

$$RT \ln \gamma_1^* = H_{01}(1 - x_1^*)^2 \quad (26)$$

and for the mixed monolayer (if component 2 is present)

$$RT \ln \gamma_1 = H_{01}(1 - x_1 - x_2)^2 + H_{12}x_2^2 + (H_{01} + H_{12} - H_{02})(1 - x_1 - x_2)x_2 \quad (27)$$

Usually for close homologues, the condition $H_{12} = 0$ can be assumed as a good approximation.²² Then it follows approximately from eq 27 that

$$RT \ln \gamma_1 = H_{01}(1 - x_1 - x_2)^2 + (H_{01} - H_{02})(1 - x_1 - x_2)x_2 \quad (28)$$

Introducing the Frumkin's constants $a_1 = H_{01}/RT$ and $a_2 = H_{02}/RT$, one obtains expressions for the activity coefficients of component 1 in the single and mixed monolayers

$$\gamma_1^* = \exp(a_1(1 - x_1^*)^2) \quad (29)$$

$$\gamma_1 = \exp(a_1(1 - x_1 - x_2)^2 + (a_1 - a_2)(1 - x_1 - x_2)x_2) \cong \exp(a_1(1 - x_1 - x_2)^2) \quad (30)$$

The approximate equality in eq 30 corresponds to the case when the values of a_1 and a_2 are roughly the same; for the more general case, $a_1 > a_2$. Similarly, one obtains for component 2 in the mixed monolayer

$$\gamma_2 = \exp(a_2(1 - x_1 - x_2)^2 + (a_2 - a_1)(1 - x_1 - x_2)x_1) \cong \exp(a_2(1 - x_1 - x_2)^2) \quad (31)$$

The commencement of the aggregation corresponds to a certain activity of the insoluble component in the single monolayer or the sum of the activities of insoluble and soluble components in the mixed monolayer. Therefore, instead of eq 24 or 25, it holds

$$x_1^*\gamma_1^* = x_1\gamma_1 + x_2\gamma_2 \quad (32)$$

Taking into account eqs 29–31, one obtains

$$x_1 = x_1^* \exp k_1 - x_2 \exp k_2 \cong x_1^* \exp k_3 - x_2 \quad (33)$$

where $k_1 = a_1(1 - x_1^*)^2 - a_1(1 - x_1 - x_2)^2 - (a_1 - a_2)(1 - x_1 - x_2)x_2$, $k_2 = (a_2 - a_1)(1 - x_1 - x_2)^2 + (a_2 - a_1)(1 - x_1 - x_2)x_1$, and $k_3 = a(1 - x_1^*)^2 - a(1 - x_1 - x_2)^2$. Here the approximate relation $a \cong a_1 \cong a_2$ is assumed to be valid. As for the case of homologues, the molar fractions are equal to the coverage values,²¹ and then instead of eq 25, one can obtain from eq 33 a more general equation

$$\theta_{cm} = \theta_c \exp k_1 - \theta_2 \exp k_2 \cong \theta_c \exp k_3 - \theta_2 \quad (34)$$

where $k_1 = a_1(1 - \theta_c)^2 - a_1(1 - \theta_{cm} - \theta_2)^2 - (a_1 - a_2)(1 - \theta_{cm} - \theta_2)\theta_2$, $k_2 = (a_2 - a_1)(1 - \theta_{cm} - \theta_2)^2 + (a_2 - a_1)(1 - \theta_{cm} - \theta_2)(\theta_{cm} + \theta_2)$, and $k_3 = a(1 - \theta_c)^2 - a(1 - \theta_{cm} - \theta_2)^2$. It is seen that, in contrast to eq 25, the nonideality of enthalpy gives rise to exponential factors at two (or one for $a_1 \cong a_2$) terms in the right-hand side of eq 34. Here the increase in θ_2 results in a less pronounced decrease of θ_{cm} , as compared with eq 25. Also, the dependence of θ_{cm} on θ_2 becomes more complicated. It should be noted that also eq 34 is an approximate relation, because it was assumed that $H_{12} = 0$, and the nonideality of entropy in the mixed monolayer was disregarded.

Adsorption of the Soluble Component in the Compressible Mixed Monolayer. Consider the dilation deformation at a constant rate of a mixed monolayer, which was first brought into equilibrium with the solution of component 2. The equation describing the balance of the soluble amphiphile in the monolayer is

$$\frac{d\Gamma_2}{dt} = -\Gamma_2 \frac{d \ln A}{dt} - D \frac{c(0,t) - c^*}{\delta} \quad (35)$$

where D is the diffusion coefficient, t is the time, $c(0,t)$ and c^* are the surface and bulk concentrations of the component 2, respectively, and δ is the thickness of the diffusion boundary layer. It is convenient to express the concentrations in eq 35 via corresponding adsorptions. The $c(0,t)$ value is determined by arbitrary coverage values of θ_1 and θ_2 and can be expressed by the adsorption isotherm equation, as long as the diffusion adsorption/desorption mechanism is assumed. Therefore, for models I and II, throughout the whole range of the area per one molecule of the insoluble homologue, the equation

$$c(0,t) = \frac{\theta_2}{b(1 - \theta_1 - \theta_2)} \quad (36)$$

which follows from eq 10, can be used, whereas for model III in the precritical range ($A \geq A_{cm}$), the equation

$$c(0,t) = \frac{1}{b} \left(\frac{\theta_2}{1 - \theta_1 - \theta_2} \right)^{1/1-\theta_1} \exp \left[\frac{\theta_2}{(1 - \theta_1)(1 - \theta_1 - \theta_2)} \right] \quad (37)$$

which follows from eq 18, is valid. The concentration in the bulk solution c^* can be expressed via the adsorption in the single solution using the adsorption isotherm equation (eq 2) for models I and II

$$c^* = \frac{\theta_2^*}{b(1 - \theta_2^*)} \quad (38)$$

or eq 19 for model III

$$c^* = \frac{1}{b} \frac{\theta_2^*}{(1 - \theta_2^*)} \exp \left(\frac{\theta_2^*}{1 - \theta_2^*} \right) \quad (39)$$

The δ value can be approximately expressed as $\delta = (D\pi t)^{1/2}$.³⁹ Noting that $dA/dt = \alpha$ and $t = \alpha(A - A_0)$ and making corresponding substitutions, one obtains for models I and II the differential equation which is valid throughout the whole A range

$$d\theta_2 = -\frac{\theta_2}{A} dA + \frac{\omega_2}{b} \left(\frac{D}{\pi\alpha(A - A_0)} \right)^{1/2} \left(\frac{\theta_2}{1 - \theta_1 - \theta_2} - \frac{\theta_2^*}{1 - \theta_2^*} \right) dA \quad (40)$$

For model III, different equations for $d\theta_2/dA$ in the precritical and transcritical range should be used:

for $A \geq A_{cm}$

$$d\theta_2 = -\frac{\theta_2}{A} dA + \frac{\omega_2}{b} \left(\frac{D}{\pi\alpha(A - A_0)} \right)^{1/2} \left[\left(\frac{\theta_2}{1 - \theta_1 - \theta_2} \right)^{1/1-\theta_1} \exp \left[\frac{\theta_2}{(1 - \theta_1)(1 - \theta_1 - \theta_2)} \right] - \frac{\theta_2^*}{1 - \theta_2^*} \exp \left(\frac{\theta_2^*}{1 - \theta_2^*} \right) \right] dA \quad (41)$$

and for $A \leq A_{cm}$

$$d\theta_2 = -\frac{\theta_2}{A} dA + \frac{\omega_2}{b} \left(\frac{D}{\pi\alpha(A - A_0)} \right)^{1/2} \left[\left(\frac{\theta_2}{1 - \theta_1 - \theta_2} \right)^{(1-\theta_1+\theta_{1c})/(1-\theta_1)} \exp \left[\frac{\theta_2(1 - \theta_1 + \theta_{1c})}{(1 - \theta_1)(1 - \theta_1 - \theta_2)} \right] - \frac{\theta_2^*}{1 - \theta_2^*} \exp \left(\frac{\theta_2^*}{1 - \theta_2^*} \right) \right] dA \quad (42)$$

Equations 40–42 can be integrated numerically for the compressible monolayer ($\alpha < 0$, $dA < 0$, $A - A_0 < 0$) throughout the range of area per molecule of the insoluble amphiphile: from the initial value $A = A_0$ to the final value $A = A$ provided that $\theta_2 = \theta_2^*(1 - \Omega_1/A_0)$ for $A = A_0$. Each of eqs 40–42 has two exact solutions for the cases of infinitely large and infinitely small compression rate of the monolayer. Consider here eq 40 as an example. For $\alpha \rightarrow 0$, equilibrium is established between the subsurface layer and the bulk, so it follows from eq 40 that

$$\theta_2 = \theta_2^*(1 - \Omega_1/A) \quad (43)$$

On the contrary, for very rapid monolayer compression (it is assumed that at $t = 0$ and $A = A_0$ the monolayer exists in the equilibrium state), the mass of the component 2 in the monolayer remains constant (desorption does not take place). Therefore, assuming $\theta_2 + \Omega_1/A < 1$, one obtains from eq 40

$$\theta_2 = \theta_2^* \frac{(1 - \Omega_1/A_0)^2}{(1 - \Omega_1/A)} \quad (44)$$

It is seen that, although according to eq 43 adsorption of the soluble amphiphile decreases during the compression of the monolayer, according to eq 44, the rapid compression results in an increase of adsorption, and this adsorption can even exceed the θ_2^* value.

Experimental Section

Materials. The tailored amphiphiles *N*-decyl- γ -hydroxybutyric acid amide ($C_{10}H_{21}-NH-CO-CH_2-CH_2-CH_2OH$, $C_{10}NH$) and *N*-tetradecyl- γ -hydroxybutyric acid amide ($C_{14}H_{29}-NH-CO-CH_2-CH_2-CH_2OH$, $C_{14}NH$) were synthesized by reaction of butyrolactone with decylamine and tetradecylamine, respectively, dissolved in dioxane at 100 °C. The chemical purity of $\geq 99\%$ obtained by distillation and crystallization in acetone was checked by elemental analysis and HPLC. The spreading solvent was chloroform p.a. (Merck). The distilled water was made ultrapure by a Milli-Q system.

Methods and Procedure. The penetration experiments were performed by using the sweeping technique. The penetration principle of this technique is based on the idea that in a multicompartment trough a Langmuir monolayer enclosed between two movable barriers and kept at selected conditions can be swept over subphases of different composition.

The circular setup used for the penetration experiments was described in detail elsewhere.^{16,20} The surface tension of the computer-interfaced film balance was measured by the Wilhelmy technique. Using a roughened glass plate, the accuracy of the surface pressure was to within 0.1 mN m⁻¹, and the time resolution was ≤ 1 s. Imaging of the monolayer was performed with a Brewster angle microscope BAM 2 (NFT, Göttingen, Germany) coupled with the penetration trough. A green laser (Uniphase, San Jose, CA) was used in the BAM. The microscope was equipped with a special scanning technique for providing sharp images. BAM images real in scale and angle were obtained by tilting the CCD sensor of the camera.

For the presented penetration experiments, the trough was partitioned in two semicircular regions. $C_{14}NH$ was spread between the movable barriers at the surface of one region filled with pure water, whereas the other region was filled with the $C_{10}NH$ solution. Hence, the two components can be characterized independent of each other. Afterward, the monolayer was brought to the desired state, e.g., molecular area, and swept onto the region containing the $C_{10}NH$ solution. The compression isotherms of the mixed monolayer for different $C_{10}NH$ concentrations were recorded with a compression rate of 0.08 nm²/ (molecule min) after equilibrating both components in the expanded monolayer state.

Results and Discussion

We consider first the results obtained for the single-component monolayers of the soluble *N*-decyl- γ -hydroxybutyric acid amide ($C_{10}NH$, component 2) and the insoluble *N*-tetra-

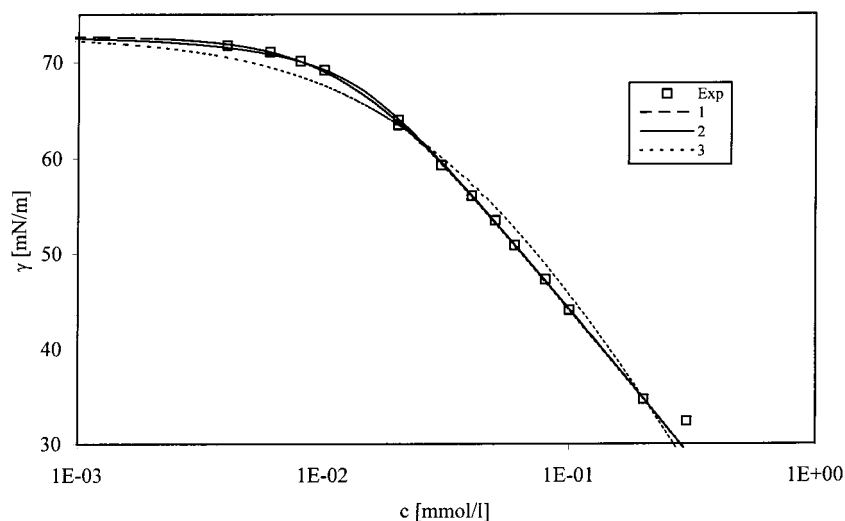


Figure 1. Dependence of the surface tension for $C_{10}NH$ vs c (\square). Theoretical isotherms were calculated from the aggregation model (curve 1) with $\omega = 1.70 \times 10^5 \text{ m}^2/\text{mol}$, $\Gamma_c = 3 \times 10^{-10} \text{ mol}/\text{m}^2$, $n = 2$, and $b = 1.02 \text{ l}/\text{mM}$, Frumkin's model (curve 2) with $\omega = 1.74 \times 10^5 \text{ m}^2/\text{mol}$, $a = 1.28$, and $b = 20.7 \text{ L}/\text{mM}$, Langmuir model (curve 3) with $\omega = 1.26 \times 10^5 \text{ m}^2/\text{mol}$ and $b = 30.6 \text{ L}/\text{mM}$.

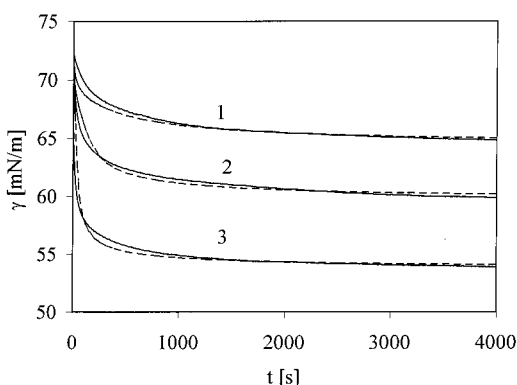


Figure 2. Dynamic surface tension for $C_{10}NH$ solutions at concentrations of 0.02 (curves 1), 0.03 (curves 2), and 0.05 mM (curves 3). Solid lines, experiment; dotted lines, calculations from the diffusion model.

decyl- γ -hydroxybutyric acid amide ($C_{14}NH$, component 1). Figure 1 illustrates the equilibrium surface tension of the aqueous $C_{10}NH$ solution at 20 °C. The theoretical curves were calculated for the Frumkin, Langmuir and aggregation models. The model parameters are listed in the legend to Figure 1. Note that, of the three models used, the best agreement with the experimental data was obtained for the aggregation model; the Frumkin model gives somewhat worse correspondence (the discrepancy between the theoretical and experimental Π values is 50% higher than that for the aggregation model), whereas the Langmuir model yields only approximate agreement with the experiment (the discrepancy is 10 times higher as compared with the aggregation model). However, to analyze the behavior of mixed monolayers, we employ here the Langmuir model, not accounting for the effect of nonideality or aggregation of $C_{10}NH$ on the surface pressure.

The dynamic surface tension of aqueous $C_{10}NH$ solutions for certain concentration values is illustrated in Figure 2. The theoretical curves shown in Figure 2 were calculated from the Ward-Tordai equation^{39,40} with eq 2 employed as the boundary condition; that is, the diffusion model for the adsorption kinetics was used. It is seen that a good correspondence exists between the theory and experiment for a reasonable value of the diffusion coefficient of $D = 4 \times 10^{-10} \text{ m}^2/\text{s}$. This fact is of a paramount importance for the subsequent analysis, because the diffusion

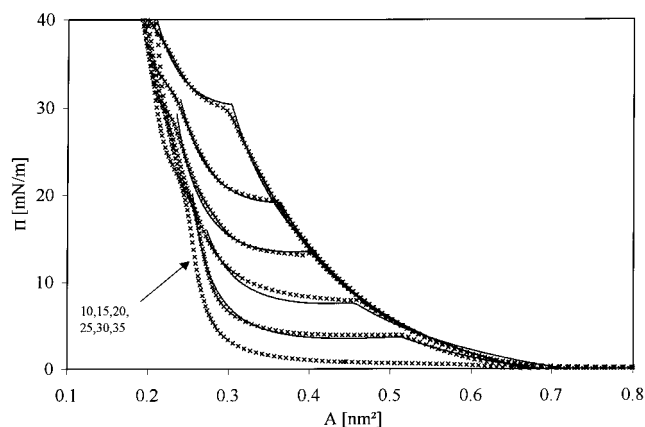


Figure 3. Experimental and theoretical $\Pi - A$ isotherms for $C_{14}NH$ at various temperatures (shown at the curves). Solid lines, experiment; dotted lines, calculations. The values of the parameters in eqs 6–8 are shown in Table 1.

TABLE 1: Values of the Equilibrium Parameters of Eqs 6–8 for $C_{14}NH$ Monolayers

temp, °C	A_c , nm ²	Ω_1 , nm ²	Π_{coh} , mN/m	ϵ
15	0.520	0.22	9.20	0.00
20	0.460	0.21	8.50	0.00
25	0.404	0.21	8.40	0.04
30	0.358	0.20	8.14	0.08
35	0.306	0.19	6.76	0.15

mechanism was assumed for the adsorption of component 2 and correspondingly, for the derivation of eqs 40–42.

The $\Pi - A$ isotherms of $C_{14}NH$ monolayers at different temperatures are shown in Figure 3. Here an excellent correspondence exists between the theoretical curves calculated from eqs 6–8 using the parameters listed in Table 1 and the experimental data. It is seen that, as usual, A_c increases with the temperature, with simultaneous decrease of Π_{coh} .

Figure 4 illustrates the experimental compression isotherms of mixed monolayers for different $C_{10}NH$ concentrations in the adjacent monolayer at 20 °C. Note that in all experiments the initial area value per one $C_{14}NH$ molecule in the monolayer was 1.3 nm², and before the monolayer compression with a constant rate of $-dA/dt = -\alpha = 0.0013 \text{ nm}^2/\text{s}$, the monolayer was allowed to stand during 5000 s after the insoluble monolayer was transferred onto the $C_{10}NH$ solution. Therefore, equilibrium

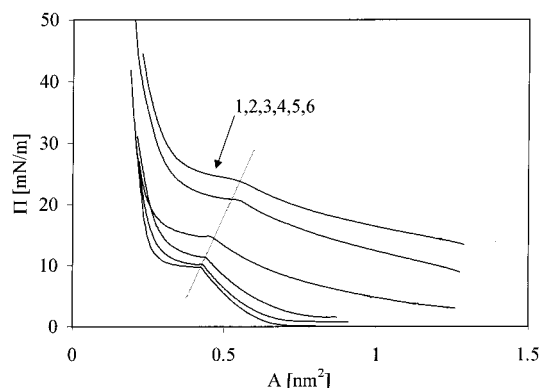


Figure 4. Experimental $\Pi - A$ isotherms for the compression ($-dA/dt = 0.0013 \text{ nm}^2/\text{s}$) of mixed monolayers of C_{10}NH and C_{14}NH at 20°C and the C_{10}NH concentrations 0.05 (curve 1), 0.02 (2), 0.01 (3), 0.002 (4), 0.001 (5), and 0.0 mM (6).

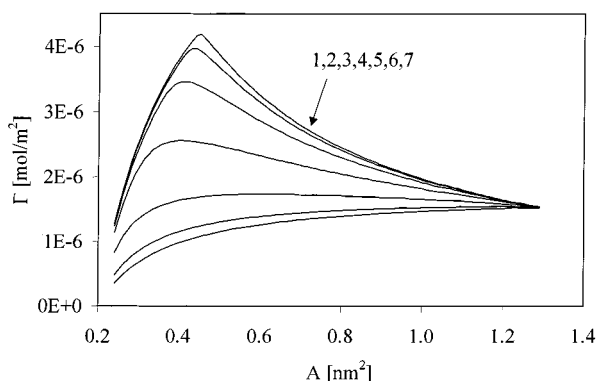


Figure 5. Dependence of C_{10}NH adsorption in mixed monolayer on A for the C_{10}NH concentration 0.01 mM and $-dA/dt = 10$ (curve 1), 1.0 (2), 0.1 (3), 0.01 (4), 0.001 (5), 0.0001 (6), and $0.00001 \text{ nm}^2/\text{s}$ (7).

of the soluble component 2 between the solution and the surface layer existed before the commencement of the compression process. It is seen from Figure 4 that in the precritical range the compression of the mixed monolayer is accompanied by an increase in the surface pressure. This implies that adsorption equilibrium does not exist for C_{10}NH , because for the equilibrated monolayer the curve for $A > 0.7 \text{ nm}^2$ should be a straight line parallel to the abscissa axis, cf. eq 13. Another important experimental result is the shift of the critical area per molecule corresponding to the commencement of the C_{14}NH condensation toward the higher values as compared to that characteristic for the single monolayer, as illustrated by the dotted line in Figure 4. It is seen that this shift becomes more significant with the increase of C_{10}NH concentration in the solution adjacent to the monolayer. This is indicative of the influence of C_{10}NH on the C_{14}NH aggregation equilibrium.

Following this, the results presented in Figure 4 are discussed in more details using the theory presented above. Consider first the influence of the compression rate of the mixed monolayer on the C_{10}NH adsorption. The dependencies shown in Figure 5 were calculated from eq 40, i.e., for the Langmuir behavior of C_{10}NH in the monolayer. All of these curves correspond to a 0.01 mM C_{10}NH solution concentration. It is seen that for very low compression rates the decrease in the area per C_{14}NH molecule leads to a decrease of the C_{10}NH adsorption. Note that curve 7 in Figure 5 is almost coincident with the dependence calculated from eq 43, that is, for equilibrium conditions of the adsorption. With the increase in the monolayer compression rate, the Γ_2 adsorption becomes higher as compared with the equilibrium value. Here for very high compression rates, an

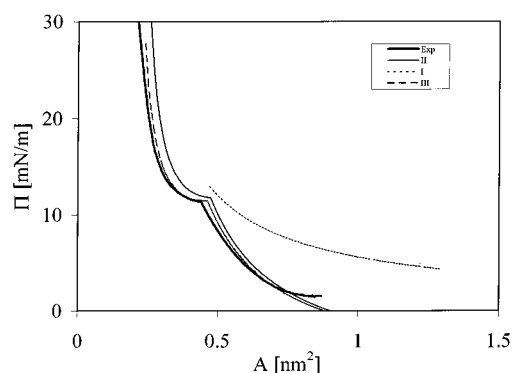


Figure 6. Experimental (bold solid line) $\Pi - A$ isotherms of the compression of mixed monolayer ($-dA/dt = 0.0013 \text{ nm}^2/\text{s}$ and $c = 0.002 \text{ mM}$) compared with theoretical dependencies calculated for the models I, II, and III.

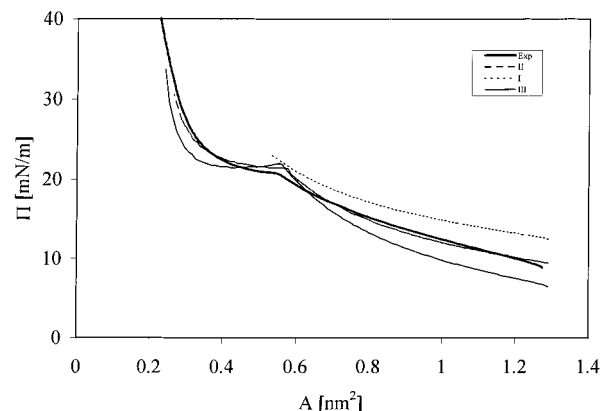


Figure 7. Experimental (bold solid line) $\Pi - A$ isotherms at the compression of the mixed monolayer ($-dA/dt = 0.0013 \text{ nm}^2/\text{s}$ and $c = 0.02 \text{ mM}$) compared with theoretical dependencies calculated for the models I, II, and III.

TABLE 2: Values of the Equilibrium Adsorption Γ_2^* and Adsorption $\Gamma_{2(\text{cm})}$ at $A = A_{\text{cm}}$ Calculated from Models I and II, Eq 40

c, mM	0.001	0.002	0.01	0.02	0.05
$\Gamma_{2(\text{cm})}, \text{mol/m}^2$	3.0×10^{-7}	5.7×10^{-7}	1.8×10^{-6}	2.56×10^{-6}	3.4×10^{-6}
$\Gamma_2^*, \text{mol/m}^2$	2.4×10^{-7}	4.8×10^{-7}	1.8×10^{-6}	3.0×10^{-6}	4.7×10^{-6}

extreme behavior of Γ_2 is indicated. Note that in the θ_2 and A ranges which satisfy the condition $\theta_2 + \Omega_1/A < 1$, curve 1 in Figure 5 coincides with the values calculated from eq 44. Our experimental conditions almost correspond to curve 5 in Figure 5. It is seen that, because of the quite high monolayer compression rate, in our experiments, the C_{10}NH adsorption was higher than the equilibrium value. This explains the increase in the surface pressure of the compressed monolayer in the precritical range, shown in Figure 4. It was mentioned above that the calculations illustrated in Figure 5 were performed for a fixed C_{10}NH concentration. The changes in the concentration of amphiphile 2 affect significantly the shape of the $\Gamma_2 - A$ curves. For a fixed α value (as in our experiments, $\alpha = -0.0013 \text{ nm}^2/\text{s}$) at $<0.005 \text{ mM}$ C_{10}NH concentrations, an increase of Γ_2 in the compressed monolayer was observed. On the contrary, for $>0.02 \text{ mM}$ concentrations, the adsorption decreases as compared with the initial value corresponding to $A = 1.3 \text{ nm}^2$. A similar behavior of the dependencies on α and c was found for the Γ_2 values calculated from eq 41.

In Figures 6 and 7, the experimental isotherm at compression of the mixed monolayer for concentrations of the soluble

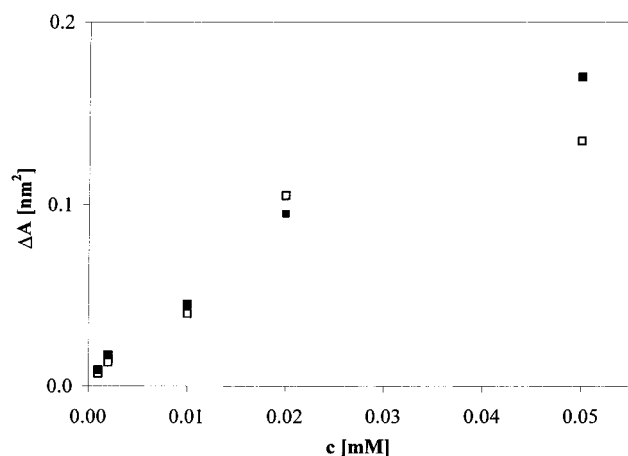


Figure 8. Theoretical dependence of $\Delta A = A_{cm} - A_c$ on the $C_{10}NH$ concentration (■) compared with the experimental data (□).

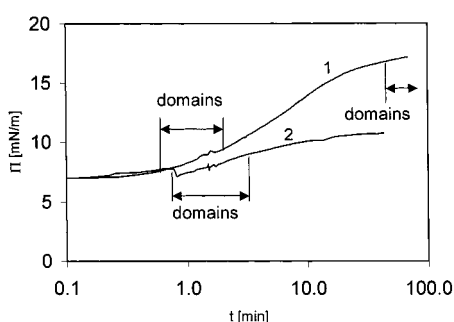


Figure 9. Dynamics of $C_{10}NH$ penetration at concentrations 0.01 (curve 1) and 0.005 mM (curve 2) at 20 °C into the $C_{14}NH$ monolayer for the initial value $\Pi = 7.0$ mN/m.

component of 0.002 and 0.02 mM, respectively, are compared with the theoretical curves calculated from the three models. For model I, the calculations were performed for the precritical A range only. It can be easily seen from the comparison between the theoretical and experimental results for a 0.002 mM $C_{10}NH$ concentration (equilibrium adsorption Γ_2^* is approximately 4.8×10^{-7} mol/m²), cf. Figure 6, that the Langmuir model I is, quite expectably, irrelevant for low concentrations (adsorptions) of amphiphile 2. At the same time, the agreement with the combined Langmuir–Volmer model II and the Volmer–Pethica model III is quite satisfactory in many details. On the contrary, for high $C_{10}NH$ concentrations in the solution (Figure 7, equilibrium adsorption Γ_2^* is approximately 4.7×10^{-6} mol/m²), all three models are in a satisfactory agreement with each other, but the best correspondence with the experiment is observed for model III. For all other concentration values

illustrated in Figure 4, the best agreement with the experiment has been also found for the models II and III.

In the mixed monolayer at $A = A_{cm}$, the $C_{10}NH$ adsorption values were calculated from model II. The corresponding dependence of $\Gamma_{2(cm)}$ on the concentration c in the solution is shown in Table 2. Here, also the Γ_2^* values obtained from the Langmuir isotherm, eq 2, are listed. The $\Gamma_{2(cm)}$ values were then used to estimate θ_{cm} from the exact eq 34, where $a_1 = 2.0 \pm 0.2$ and $a_2 = 1.3$ was assumed, cf. Figure 1. It is known that the value $a_1 = 2$ corresponds to the critical value of the Frumkin equation of state and isotherm. The agreement between the experimental data, shown in Figure 4, and the theoretical values of the critical area A_{cm} per one $C_{14}NH$ molecule in the mixed monolayer is rather good, see Figure 8. The A_{cm} values calculated from the approximate eq 34 for $a = 2 \pm 0.1$ are close to the results obtained from the exact calculations. However, disregarding the activities in the mixed monolayer, that is, applying eq 25 instead of eq 34, leads to an increase of the critical area value approximately 2–3 times higher than that observed in the experiment.

Figure 9 illustrates the dynamic surface pressure of mixed monolayers at 20 °C during the penetration of $C_{10}NH$. The initial state of the $C_{14}NH$ monolayer was taken close to the critical state; that is, the surface pressure was 1 mN/m lower and the area per one $C_{14}NH$ molecule was 0.02 nm² higher than the values which correspond to the commencement of condensation at the given temperature in the single pure monolayer, see Figure 3. Therefore, in the initial state, the monolayer does not contain aggregates. The penetration of $C_{10}NH$ results in the fact that, when the surface pressure increases to ~ 8 mN/m (which approximately corresponds to $\theta_2 \approx 0.03$), in the two solutions studied, aggregation in the form of condensed phase domains occurs which vanish with time at higher pressures. The ranges of the existence of the domains are shown by the arrows in Figure 9. For the $C_{10}NH$ solution with a concentration of 0.005 mM, further adsorption results in a small pressure increase; this, however, did not lead to any aggregation in the monolayer. On the contrary, for the $C_{10}NH$ solution with a concentration of 0.01 mM at time values exceeding 50 min, the formation and growth of domains was again observed (shown by the double arrow in Figure 9). The condensed phase domains formed both in the transient region and in the stable state at high solute concentration can be visualized by BAM. The morphology of the crystalline domains is similar to each other in both states and resembles that of the pure $C_{14}NH$ monolayers (Figure 10).

In the case of the second region of stable condensed phase domain formation, the initial point of domain formation corresponds to a value of $\theta_2 = 0.12$. The calculations according to eq 34 have shown that for $\theta_2 = 0.12$ the shift of critical area

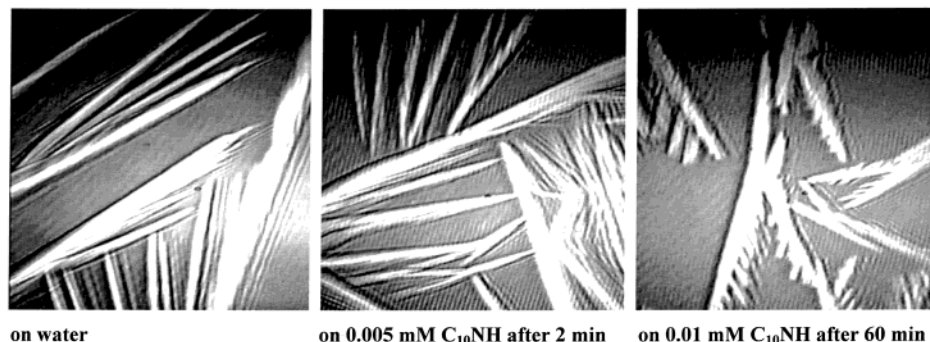


Figure 10. BAM images on the dynamics of $C_{10}NH$ penetration into the $C_{14}NH$ monolayer for an initial value $\Pi = 7.0$ mN/m. Similarity of the condensed phase domains of pure $C_{14}NH$ monolayers on water (left), of transient domains formed at the beginning of the $C_{10}NH$ penetration, and of stable condensed phase domains formed at high $C_{10}NH$ concentrations near the penetration equilibrium. $T = 20$ °C; image size 450×450 μ m.

value ($A_{\text{cm}} - A_c$) per one C_{14}NH molecule is 0.02 nm^2 (or $\theta_c - \theta_{\text{cm}} \cong 0.02$), which is exactly equal to the difference of $A - A_c$ before the penetration. Thus, eq 34 is in a perfect agreement with the experiment for the second range of the existence of stable domains shown in Figure 9.

Next the possible mechanism of formation and disappearance of the domains in the first region in Figure 9 is discussed. Equation 34 holds for the equilibrium state of the monolayer. For a rapid penetration process (it is seen from Figure 9 that the domains are formed within 30 s), the equilibrium state, i.e., perfect ordering of all molecules in the monolayer, is unlikely to occur. For these conditions, one can suppose that the state of mixed monolayer is close to the ideal state. In this case, eq 25 can be used to estimate the shift in the critical area value of C_{14}NH in the mixed monolayer. Quite surprisingly, the decrease in the monolayer coverage by the insoluble amphiphile, which is necessary for the formation of domains, $\theta_c - \theta_{\text{cm}} = 0.02$, and equal to θ_2 according to eq 25, is almost the same as the value of C_{10}NH adsorption estimated above for the beginning of the range where instable domains are formed, ($\theta_2 \cong 0.03$). According to the conditions necessary to achieve the equilibrium intermolecular interaction, the relaxation time for mixed monolayer should be of the order of 100 s. This can explain the subsequent disappearance of the domains 2–4 min after the commencement of the penetration process.

Conclusions

Equations of state for mixed monolayers of an insoluble and a soluble homologues and the adsorption isotherm equation for soluble amphiphile are derived for some theoretical models on the basis of the generalized Szyszkowski–Langmuir, Volmer, and Pethica equations and on combinations of these models. Assuming diffusion kinetics for the desorption of the soluble component during the compression of the mixed monolayer, an equation is derived for the surface concentration (adsorption) of the soluble amphiphile. The dependence of this value on the conditions of the monolayer compression, concentration, and other parameters can be analyzed. The influence of the non-ideality of mixture on the shift of the area value per molecule of the insoluble amphiphile, which corresponds to the commencement of the two-dimensional condensation in the monolayer, is theoretically treated.

Single-component and mixed monolayers of the soluble *N*-decyl- γ -hydroxybutyric acid amide ($\text{C}_{10}\text{H}_{21}\text{—NH—CO—CH}_2\text{—CH}_2\text{—CH}_2\text{OH}$, C_{10}NH , component 2) and the insoluble *N*-tetradecyl- γ -hydroxybutyric acid amide ($\text{C}_{14}\text{H}_{29}\text{—NH—CO—CH}_2\text{—CH}_2\text{—CH}_2\text{OH}$, C_{14}NH , component 1) are studied experimentally, and the results are compared with theoretical predictions. The theory is found to be in a satisfactory agreement with the experiment. It is shown that the account for the nonideality in the mixture of amphiphiles is important for the qualitative and quantitative analysis of the formation of domains in the mixed monolayer.

The theoretical model of the compressible mixed monolayer proposed here is important in a general sense and can be applied to other compression/expansion processes in biology and technology.

Acknowledgment. The work was financially supported by the Max Planck Society and by the Ukraine SFFR (03.07/00227). We thank Dr. R. Wagner for the preparation of the amphiphiles.

References and Notes

- Pethica, B. A. *Trans. Faraday Soc.* **1955**, *51*, 1402.
- Anderson, P. J.; Pethica, B. A. *Trans. Faraday Soc.* **1956**, *52*, 1080.
- McGregor, M. A.; Barnes, G. T. *J. Colloid Interface Sci.* **1976**, *54*, 439; **1977**, *60*, 408.
- Alexander, D. M.; Barnes, G. T. *J. Chem. Soc., Faraday Trans. 1* **1980**, *76*, 118.
- Motomura, K.; Hayami, I.; Aratono, M.; Matuura, R. *J. Colloid Interface Sci.* **1982**, *87*, 333.
- Panaiotov, I.; Ter-Minassian-Saraga, L.; Albrecht, G. *Langmuir* **1985**, *1*, 395.
- Ter-Minassian-Saraga, L. *Langmuir* **1985**, *1*, 391.
- Hall, D. G. *Langmuir* **1986**, *2*, 809.
- Tajima, K.; Koshinuma, M.; Nakamura, A. *Langmuir* **1991**, *7*, 2764.
- Jiang, Q.; O'Lenick, C. J.; Valentini, J. E.; Chiev, I. C. *Langmuir* **1995**, *11*, 1138.
- Asano, K.; Miyano, K.; Ui, H.; Shimomura, M.; Ohta, I. *Langmuir* **1993**, *9*, 3587.
- Vollhardt, D.; Wittig, M. *Colloids Surf.* **1990**, *47*, 233.
- Siegel, S.; Vollhardt, A. D. *Colloids Surf.* **1993**, *76*, 197.
- Sundaram, S.; Stebe, K. J. *Langmuir* **1996**, *12*, 2028; **1997**, *13*, 1729.
- Santos Magalhaes, N. S.; de Oliveira, H. M.; Baszkin, A. *Colloid Surf. A* **1996**, *118*, 63.
- Sundaram, S.; Ferri, J. K.; Vollhardt, D.; Stebe, K. J. *Langmuir* **1998**, *14*, 1208.
- Fainerman, V. B.; Vollhardt, D. *Langmuir* **1999**, *15*, 1784.
- Fainerman, V. B.; Makievski, A. V.; Vollhardt, D.; Siegel, S.; Miller, R. *J. Phys. Chem. B* **1999**, *103*, 330.
- Fainerman, V. B.; Zhao, J.; Vollhardt, D.; Makievski, A. V.; Li, J. B. *J. Phys. Chem. B* **1999**, *103*, 8998.
- Vollhardt, D.; Fainerman, V. B. *Adv. Colloid Interface Sci.* **2000**, *86*, 103.
- Fainerman, V. B.; Lucassen-Reynders, E. H.; Miller, R. *Colloids Surf. A* **1998**, *143*, 141.
- Lucassen-Reynders, E. H. In *Anionic Surfactants (Physical Chemistry of Surfactant Action)*; Lucassen-Reynders, E. H., Ed.; Marcel Dekker Inc.: New York, 1981; p 1.
- Mulqueen, M.; Blankschtein, D. *Langmuir* **1999**, *15*, 8832.
- Nikas, Y. J.; Puvvada, S.; Blankschtein, D. *Langmuir* **1992**, *8*, 2680.
- Lu, J. R.; Thomas, R. K.; Penford, J. *Adv. Colloid Interface Sci.* **2000**, *84*, 143.
- Fainerman, V. B.; Vollhardt, D.; Emrich, G. *J. Phys. Chem. B* **2001**, *105*, 4324.
- Fainerman, V. B.; Miller, R.; Aksenenko, E. V. *J. Phys. Chem. B* **2000**, *104*, 5744.
- Frumkin, A. N. *Z. Phys. Chem. (Leipzig)* **1925**, *116*, 466.
- Ferry, J. K.; Stebe, K. J. *Colloids Surf. A* **1999**, *156*, 567.
- Ferry, J. K.; Stebe, K. J. *J. Colloid Interface Sci.* **1999**, *208*, 1.
- Fainerman, V. B.; Miller, R. *J. Phys. Chem. B* **2000**, *104*, 8471.
- Fainerman, V. B.; Miller, R. *J. Colloid Interface Sci.* **2000**, *232*, 254.
- Vollhardt, D.; Fainerman, V. B.; Emrich, G. *J. Phys. Chem. B* **2000**, *104*, 8536.
- Vollhardt, D.; Fainerman, V. B. *Colloids Surf. A* **2000**, *176*, 117.
- Fainerman, V. B.; Vollhardt, D. *J. Phys. Chem. B* **1999**, *103*, 145.
- Volmer, M. *Z. Phys. Chem. (Leipzig)* **1925**, *115*, 253.
- Hildebrand, J. H.; Scott, J. R. *Regular Solutions*; Prentice-Hall: Englewood Cliffs, New Jersey, 1962.
- Read, R. C.; Prausnitz, J. M.; Sherwood, T. K. *The Properties of Gases and Liquids*, 3rd ed.; McGraw-Hill Inc.: New York, 1977.
- Dukhin, S. S.; Kretschmar, G.; Miller, R. Dynamics of Adsorption at Liquid Interfaces: Theory, Experiment, Application. In *Studies in Interface Science*; Möbius, D., Miller, R., Eds.; Elsevier: Amsterdam, 1995; Vol. 1.
- Ward, A. F. H.; Tordai, L. *J. Chem. Phys.* **1946**, *14*, 453.